Shape of adhesive fluid controls insect adhesion in air and underwater

Pranav Sudersan,[†] Michael Kappl,[†] Thomas Endlein,[†] Bat-El Pinchasik,[‡] and Hans-Jürgen Butt[*,†]

[†]*Max Planck Institute for Polymer Research, Ackermannweg 10, 55128 Mainz, Germany*

[‡]*Tel Aviv University, Tel Aviv-Yafo, Israel*

E-mail: butt@mpip-mainz.mpg.de

Phone: +49 6131 379 111. Fax: +49 6131 379 310

Abstract

Insects ~~like beetles~~ can stick to various surfaces using hairy pads mediated by an oily adhesive fluid. The pads can even attach underwater, presumably due to an air bubble trapped around the pad. There is however a lack of understanding of the exact role of the bubble for underwater adhesion. Here, we perform *in-vivo* underwater adhesion measurements of a ~~constrained~~ ladybug pad in the presence and absence of trapped bubble and compare it with adhesion in air. Our experiments reveal that on a hydrophobic substrate, even without a bubble, the pad can show adhesion underwater comparable to that in air. Only on a hydrophilic substrate, a trapped bubble is necessary to aid adhesion underwater. To explain these results, we develop a simple theoretical model which estimates the net adhesion of a hairy pad due to capillary forces. Our results demonstrate that capillary forces in insects are primarily governed by the shape of the adhesive fluid and can help explain its adhesion in both air and underwater conditions.

1 Introduction

The question of how insects can walk on smooth surfaces against gravity has fascinated scientists for at least the past three centuries[1,2]. We now know that such animals are able to adhere by utilizing specialized organs on their feet called adhesive pads. These adhesive pads occur in a variety of types depending on the animal, but generally categorized into: 1) "smooth pads" found in ants, crickets and 2) "hairy pads" seen in flies and geckos. The hairy pad design has many advantages. They show: 1) compliance to rough surfaces due to their lower effective modulus, 2) angle dependent adhesion due to asymmetric hair geometry and 3) self-cleaning capability[3]. Many of these insects pads also secrete an adhesive fluid as seen in flies and ants[4] ("wet adhesion"), while some such as spiders and geckos rely on their dry hairy pads for attachment ("dry adhesion"). In the "wet adhesion" case, fluid secretion can facilitate adhesion through surface tension and viscous forces[5], on the other hand dry adhesion" relies mostly on van der Waals forces[6].

Most terrestrial beetles such as the dock beetle or ladybug have hairy pads consisting of a dense array of hair like structures called setae. The setae tips have a distribution of geometries such as discoidal, spatula or pointed shaped depending on the pad, sex and species[7]. Single seta force measurements reveal that discoidal shaped seta show larger pull-off force than spatula and pointed setae[8], illustrating the role of hair geometry on adhesion. The tip of each seta secretes approximately $1 \mu m^3$ of oily adhesive fluid[9], whose chemical composition is identified as a mixture of mostly long chain hydrocarbons[10] with traces of triglycerides, fatty acids and cholesterol[11,12]. A recent study[13] based on an elastocapillary model has been able to reasonably predict single seta adhesion forces theoretically, confirming the dominant role of surface tension in the "wet adhesion" of beetles.

While most of the studies on insect adhesion have focused on "terrestrial" conditions in air, animal attachment underwater has been relatively unexplored. Typically, underwater adhesion is complicated to achieve due to the difficulty in displacing the water layer and enable good contact[14]. Regardless, geckos show the remarkable behavior, where

its shear adhesion force on hydrophobic substrates are similar in both air and underwater conditions. Interestingly, its adhesion on a fluorinated substrate is larger underwater than in air[15]. This has been partially explained by a thermodynamic work of adhesion model assuming full displacement of water leading to dry contact of hairs[16]. A study on leaf beetles[17] has also revealed that beetles can attach well to surfaces underwater. Its hairy pad traps an air bubble underwater which dewets the surface on contact. It has been hypothesized that a combination of capillary forces due the air bubble and direct contact of hairs within the dewetted zone results in attachment. However, a detailed investigation of this phenomenon is lacking.

The goal of this paper is to provide a general unified picture of insect adhesion in both air and underwater conditions to substrates with different wettability. We focus ~~our attention~~ towards insects with hairy pads relying on adhesive fluid for attachment. First~~ly~~, we perform adhesion measurements of a single constrained pad of a live ladybug beetle in air and underwater conditions. The experiments are performed on a smooth glass (hydrophilic) and a fluorinated ~~(hydrophobic)~~ surface with a ~~simultaneous video~~ microscopy observation of the contact process. Second~~ly~~, we develop a simple theoretical model considering capillary forces to predict the net adhesion force of a hairy pad under different conditions. Finally, we discuss key insights gained from our model and experiments as well as possible implications in understanding adhesion in other animals.

2   Experimental

Normal adhesion force measurements on a ~~restrained~~ leg of a live ladybug beetle are performed. We characterize adhesion by the pull force during detachment. Measurements are done against smooth glass and fluorinated surface to represent hydrophilic and hydrophobic substrates respectively. In underwater conditions, measurements are done both in the presence and absence of trapped bubble to investigate the bubble's role in underwater adhesion.

The three possible contact types are thus labeled as: 1) "Air", 2) "Underwater: Wet" and 3) "Underwater: Bubble".

2.1 Material and Methods

2.1.1 Substrate preparation

Standard 20 mm wide glass coverslips are used as the hydrophilic substrate. Glass was wiped with isopropanol, rinsed in water and dried under nitrogen flow. The surface was then plasma cleaned in oxygen plasma chamber (Diener Electronic Femto) for 10 mins at120 W ~~power~~. The surface was further rinsed with water and dried under nitrogen flow.

For the hydrophobic substrate, the glass cover slip was coated with a fluorosilane via chemical vapor deposition (CVD) ~~method~~. The glass was first cleaned using IPA and plasma treated as before. 0.2 ml of Trichloro(1H,1H,2H,2H-perfluorooctyl) silane (PFOTS), procured from Sigma Aldrich, was put in a sealed chamber along with the the glass cover slip. The chamber was placed under 100 mbar pressure for 10 mins for the CVD process. The glass substrates were finally annealed at 150℃ for 3 hours.

The substrate wettability was characterized by dynamic contact angle measurements performed with a DataPhysics OCA 35 contact angle goniometer using water and n-hexadecane. Advancing and receding contact angles were measured for a maximum drop volume of 10 μl and with 0.5 μl/s flow rate. Static contact angles were measured for a 5 μl drop.

Table 1: Static and dynamic contact angles measurements

Substrate	Liquid	θ_A	θ_R	θ_S
Glass	Water	63±5°	20±2°	57±
	n-Hexadecane	<10°	<10°	<10°
PFOTS	Water	122±1°	93±2°	110±2°
	n-Hexadecane	88±2°	56±5°	72±2°

2.1.2 Field desorption mass spectroscopy

Field Desorption Mass Spectrometry (FDMS) measurements of the adhesive fluid secretions were performed using ZAB 2-SE-FPD spectrometer (VG Instruments). A previous study on archanids[18] reported that the secreted fluid does not dissolve away in water. To confirm this for the beetle, measurements before and after the immersion of its legs in water were done. The middle leg of an Asian ladybird (*Harmonia axyridis*) was immersed in 50 μL THF for 20 m and then transferred to the measurement chamber of the FDMS. As a reference, pure THF was used. The second middle leg of the same ladybird was immersed in 100 μL milli-Q water for 15 minutes, then in THF for 20 minutes and then transferred to the measurement chamber of the FDMS. Molecular composition is extracted from the peak positions of the FDMS data.

2.1.3 Specimen preparation

Seven-spotted adult ladybug beetles (*Coccinella septempuctata*) purchased from Katz Biotech (Baruth, Germany) were used for adhesion tests. The beetles were housed in a plastic box filled with leaves, twigs and stones under at room temperature and 60-80% relative humidity with access to sunlight ~~to give it a close to natural habitat~~. The beetles were fed with raisins, honey and water *ad libitum*.

Experiments were done ~~only~~ on male beetles since their adhesive pads possess discoidal shaped setae capable of strong adhesion. For the test, the beetle's leg was constrained similar to the method described by Bullock et al[7]. A steel ball fixed with a piece of thick solder wire was used as a holder to fix and constrain the beetle and its leg (Figure 1). The beetle was first anesthetized using dry ice and glued to the steel ball on its back. Its front left leg was carefully fixed to the solder wire using Blue-Tac. Its claw was fixed using epoxy glue to prevent any wiggling. The leg was aligned such that only the distal pad of its leg can make contact. Teflon tape was used like a blanket to wrap around the rest of its body to prevent interference by its other legs.

After measurements, the beetle was freed by carefully removing the epoxy glue and Blue-Tac without harming it using a pair of tweezers and was finally set free to ponder about that confusing experience.

2.1.4 Adhesion test

Adhesion measurements were performed on a custom force measurement setup developed in-house (Figure 1). A fiber optic displacement sensor (Philtec D20, PHILTEC, Inc. USA) together with a steel bending beam constitutes the vertical force sensor. Beam deflection was calibrated using 4 different known weights to get the corresponding force. A plastic 3D printed substrate holder was glued to the end of the bending beam. The holder was designed to allow switching from one substrate to another without removing any glue. It "tank" like design also allows it to be filled with water for underwater tests. The sensor was mounted on a stage consisting of a X-piezo used for precise lateral movements, XYZ motors for coarse movements and goniometer for adjusting substrate alignment with the optics. Additionally, a separate Z-piezo fixed upright is used for vertical up-down motion, bringing the specimen in contact with the substrate from top. A 3 axis manual micro-manipulator together with a free stainless steel ball allowed good alignment of the beetle's foot to the substrate. A coaxial illuminated tube microscope (Navitar) with 2x objective and a stereo-microscope with 1x objective (Wild Heerbrugg) fit with cameras are used to record the sample contact with the substrate from bottom and side views respectively. The data acquisition from the force sensor and cameras together with an appropriate piezo motion steps are synchronized using a custom LABVIEW program. Force data was acquired at a sample rate of 984 Hz, averaged to 512 points per motion step. Videos were recorded at 20 frames per second.

The vertical and lateral piezos were together used to perform approach-retract adhesion tests with the substrate to get the pull-off force. However, instead of a simple down-up motion some additional motion steps were included (Figure 1 b). A 100 μm lateral sliding motion was done after the initial approach step to give a proximal pull to the beetle's leg

and thus properly orient its hairs with the substrate[7]. An additional 10 μm compression step (approach) was done to ensure all hairs are loaded and make good contact with the surface. A 1 second "Pause" step was done to minimize any viscoelastic effects before finally retracting the leg away from the substrate. All approach, retract and sliding motion was done at a speed of 62.5 μm/s. Bottom view video recordings were used for contact area extraction while the side view imaging is used only to visually aid orienting the pad with the substrate before a test. Figure 1 shows a typical measurement data where recorded force is plotted as a function of time along with the observed pad contact area extracted via image processing.

For underwater experiments, 1 ml ~~of~~ deionized water was poured into the substrate holder. In order to achieve an underwater "wet" contact, the likelihood of bubble trapping between the pad was reduced by degassing the water in a vacuum chamber for 3 hours before use.

10 contact measurements were done on the same spot of the surface to equilibriate the pad system. 5 measurements were subsequently performed on a fresh spot of the substrate for each type of contact and were used for data analysis. Experiments were repeated with 5 distinct beetles for each type of contact. In total, 30 beetles were tested.
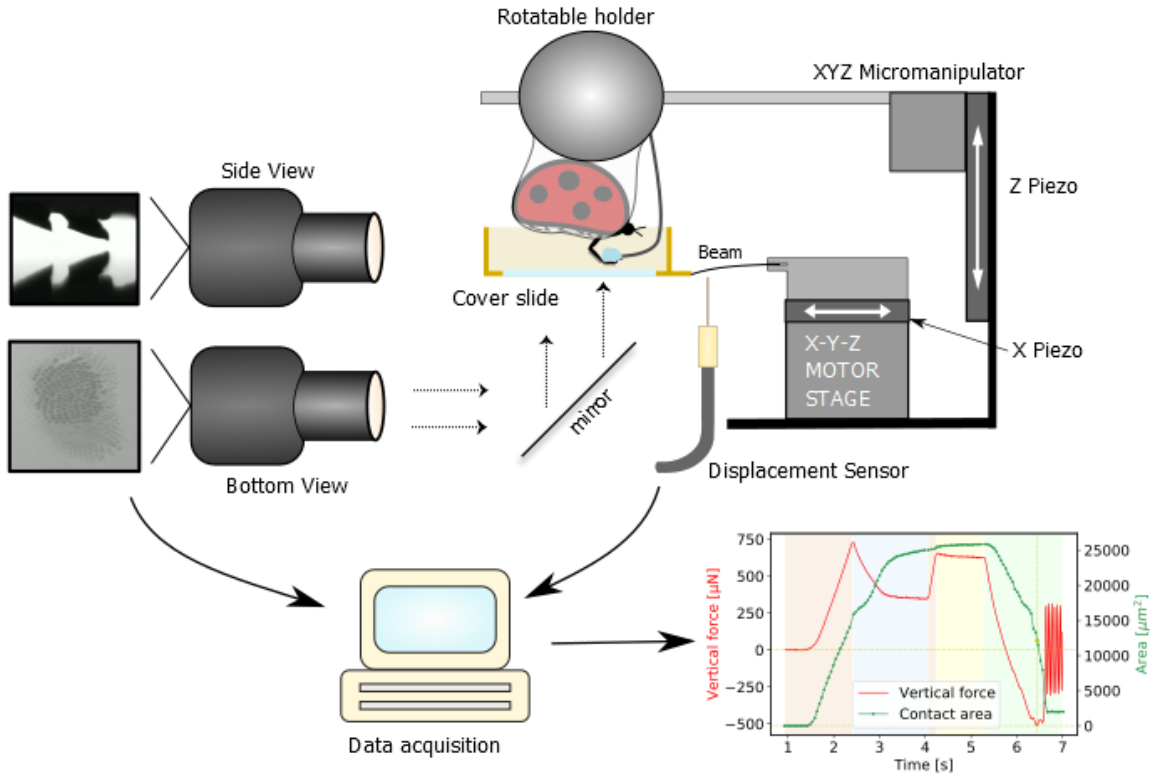
Figure 1: a) Adhesion test setup b) Representative force data and contact area of distal pad for a typical measurement. Shaded regions represent distinct motion steps. Minimum peak value during final retract step is taken as adhesion force.

2.1.5 Data analysis

Extraction of pull-off force from force data, image processing, plotting and statistical analysis were all performed in "*Buggee*"[19], a tool written in Python using open-source libraries for synchronous analysis of force data and video recordings.

For measurements in air, pull-off force is defined as the minimum force during the final retraction step. For underwater measurements, an additional correction needs to be done first. During the piezo motion, contact line of the immersed holder at water surface changes, influencing the force readout due to surface tension. This effect needs to be canceled. So, a background force data is recorded where the submerged beetle makes no contact with

8

the substrate. The background forces is then subtracted from a typical force data with substrate contact to correct for the external surface tension effects. After this, the pull-off force is calculated from the minima as before.

Data sets are compared for statistical deviations using pairwise Tukey t-test and their corresponding effect sizes are compared using Pearson correlation coefficients. Shapiro-Wilk test was done for each data sets to verify normal distribution of its residuals and Levene's test was done to check equality of the respective variances, thus validating the assumptions involved in the Tukey test.

2.2   Results

2.2.1   Field desorption mass spectroscopy

Molecular weights of secreted fluid mixtures extracted from an Asian ladybird (*Harmonia axyridis*) without (left) and with (right) immersion in water are compared (Table 2). Except from two molecular weights (406.8 g/mol and 331.6 g/mol), the chemical fingerprint remained unchanged, indicating stability of the lipid mixture underwater. Probable molecules, corresponding to the resulting molecular weights, include aliphatic hydrocarbons and aldehydes.

Table 2: Molecular weights of adhesive fluid secretion of *Harmonia axyridis* with and without rinsing the beetle's leg in water. Molecular weights correspond to peaks in the FDMS data.

Without rinsing in water (g/mol)	After immersion in water (g/mol)	Probable compounds
324.5	324.5	$C_{23}H_{48}$, $C_{22}H_{44}O$
	331.6	$C_{24}H_{44}$
350.5	350.5	$C_{25}H_{50}$
352.5	352.5	$C_{25}H_{52}$, $C_{24}H_{48}O$
378.5	378.5	$C_{27}H_{54}$
404.6	404.5	$C_{29}H_{56}$
406.8		$C_{29}H_{58}$
432.8	432.7	$C_{31}H_{60}$

2.2.2 Adhesion test

Adhesion force for the distal pad of ladybug beetle against glass and PFOTS in air and underwater conditions are compared (Figure 2). In air, there is only a small difference in the median adhesion force on glass and PFOTS. The small difference can be attributed to the higher receding contact angle of oil in PFOTS when compared to glass (Table 1). In underwater, a l⬜ difference is seen in the forces between glass and PFOTS for a wet contact. On glass, very small adhesion is recorded while P⬜TS shows an adhesion close to that in air. For a bubble contact, both glass and PFOTS show similar adhesion. Statistical significance values for comparison of the different contact types (Table 3) support the above conclusions.

Table 3: Statistical analysis of adhesion force. p-value and T are obtained from pair-wise Tukey test between A and B while keeping the third parameter fixed. r values represent the corresponding Pearson correlation coefficient

| A	B	Fixed	p-tukey	T	r
Air	Underwater: Bubble	Glass	0.211	1.95	0.298
Air	Underwater: Wet	Glass	0.001	10.985	0.846
Underwater: Bubble	Underwater: Wet	Glass	0.001	5.857	0.774
Air	Underwater: Bubble	PFOTS	0.9	0.017	0.002
Air	Underwater: Wet	PFOTS	0.854	0.767	0.085
Underwater: Bubble	Underwater: Wet	PFOTS	0.9	0.561	0.083
Glass	PFOTS	Air	0.16	1.405	0.151
Glass	PFOTS	Underwater: Bubble	0.348	-0.939	-0.192
Glass	PFOTS	Underwater: Wet	0.001	-8.258	-0.776
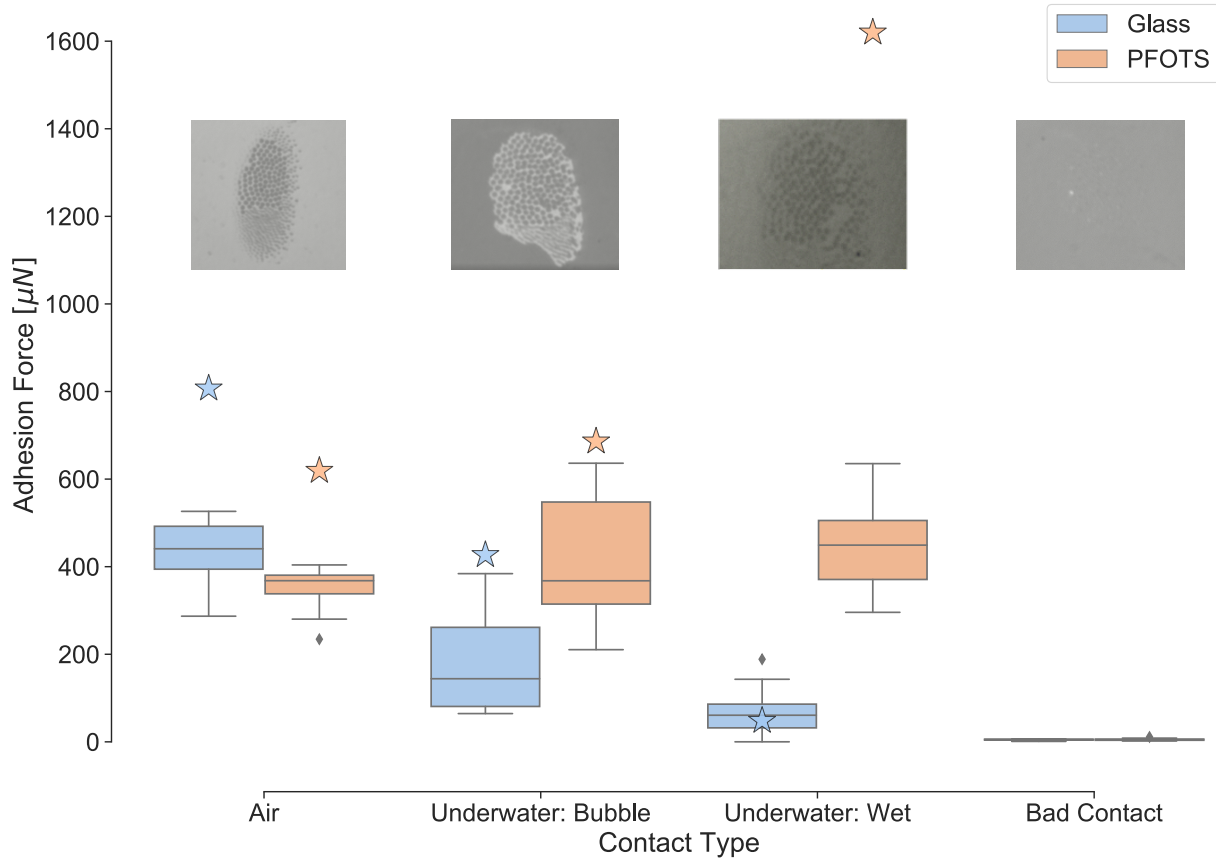
Figure 2: Adhesion force measurements of ladybug beetle on glass and PFOTS substrates in air and underwater conditions. Values represent peak force of a distal pad pulled off from each substrate at 62.5 μm/s retraction speed. Three types of contact are seen in underwater experiments and are represented separately: "Bubble", "Wet" and "Bad Contact". Insets show bottom view images of the corresponding contact types. Stars represent theoretical predictions of adhesion force calculated from Capillary Bridge Model, where hair diameter = 4 μm, pad diameter = 200 μm, hair height = 40 μm, number of hairs = 500, adhesive fluid volume = 4.2 fL and bubble volume = 1.2 nL.

Apart from the three predicted contact types, we also observed an additional fourth contact which randomly occurs underwater, labeled as "bad contact". During such a contact the bottom view contact area recordings don't show a prefect contact of hairs with the substrate as is usually seen for the other three contact types. "Bad contact" always shows no adhesion with either glass or PFOTS substrate. While it's not completely clear why such a contact occurs, there can be two possible reasons:

1. The hairs could get bundled due to a small air meniscus inside the hairs, resulting in

11

its disorientation.

2. The substrate is not dewetted during contact, causing a thin water layer on the surface to prevent adhesion.

3 Theoretical

3.1 Capillary Bridge Model

We modeled the hairy pad as an array of N cylindrical rods of length L and diameter, D_h fixed to a flat circular base of pad diameter D_p as shown in figure 3. For simplicity, we assume both hairs and the pad to be perfectly rigid. The tip of each cylindrical hair has an adhesive fluid of volume V_f making contact with the substrate. The fluid is assumed to be pinned to the circumference of the hair and forms a capillary bridge of height d with the substrate. In order to model the contact in both air and underwater conditions, we consider three types of contacts:

1. *Air contact* - All hairs and fluid bridges are surrounded by air

2. *Underwater: Wet contact* - All hairs and fluid bridges are surrounded by water

3. *Underwater: Bubble contact* - A bubble of volume V_b is trapped between the hairs. The bubble is pinned to pad circumference. Liquid bridges forming contact with the substrate within the bubble are surrounded by air while the ones forming contact outside the bubble are surrounded by water.
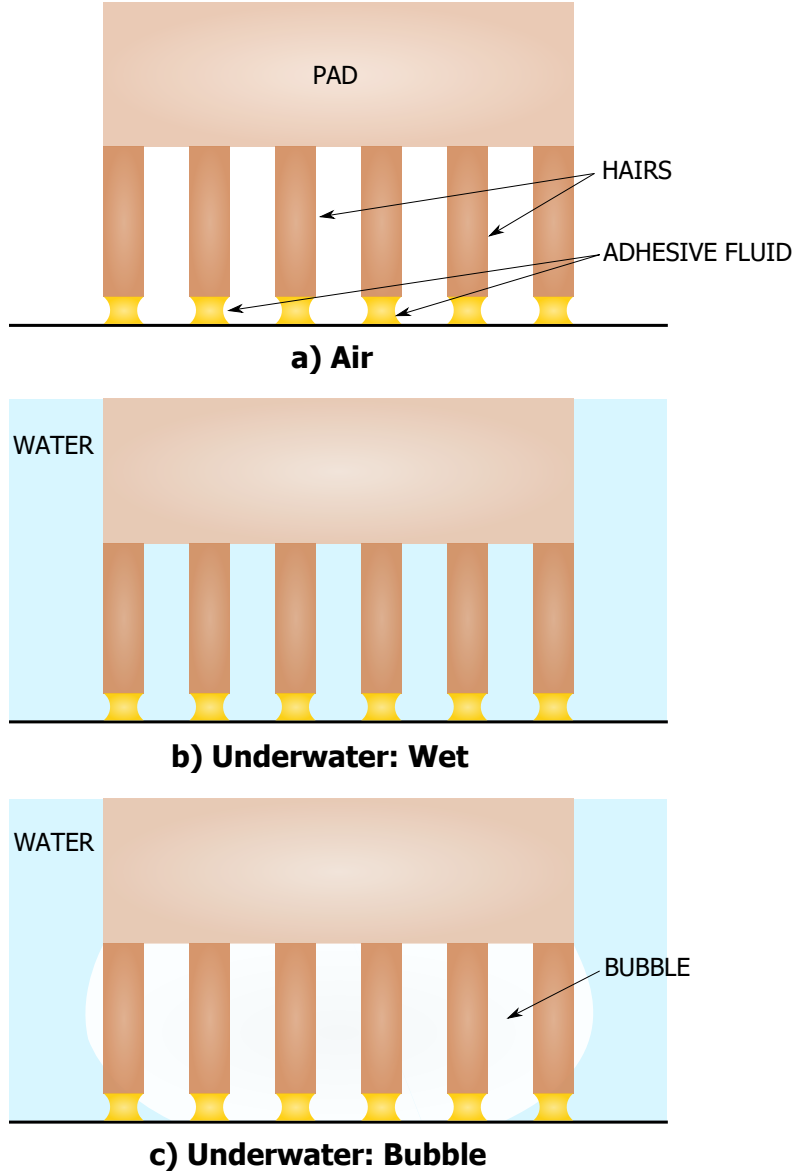
Figure 3: Capillary Bridge Model. The hairy pad system comprises of a cylindrical pad of diameter D_p acting as support for an array rigid cylindrical hairs with diameters D_h. The tip of each hair carries an adhesive fluid forming a capillary bridge with the substrate. This hairy pad makes contact with a substrate in three ways: *Air*, where the adhesive fluid bridges are surrounded by air; *Underwater: Wet*, where the adhesive fluid bridges are fully surrounded by water; *Underwater: Bubble*, where part of the adhesive fluid bridges are inside the bubble while others are outside in water. ~~The adhesive fluid size scales with D_h according to the fluid size parameter ϕ_f. The bubble size scales with D_p according to the bubble size parameter ϕ_b. Total hair area fraction (α) and aspect ratio (L/D_h) are fixed. The net force is calculated from capillary contributions due to all adhesive fluid bridges and the bubble~~

Let $V_f = 4/3\pi s_f^3$ and $V_b = 4/3\pi s_b^3$, where s_f and s_b are the radii of spheres with equivalent volumes. Fluid and bubble sizes are assumed to scale proportionally in a "self-similar" manner relative to their pinned contact size. We thus define the size parameters $\phi_f = D_f/2s_f$ and $\phi_b = D_b/2s_b$ for the fluid and bubble respectively to conveniently scale their sizes relative to the corresponding hair and pad diameters they are pinned to. The tip of the hairs are at a distance d from the the substrate.

The net adhesion force for case 1 and 2 can be calculated as:

$$F_{net} = Nf \tag{1}$$

Here, f is capillary force by a single fluid bridge at distance d, and N is the total number of hairs

For case 3, the net adhesion force is given by:

$$F_{net} = N_{in}f_{air} + N_{out}f_{water} + f_{bubble} \tag{2}$$

Here, N_{in} and N_{out} are the number of hairs inside and outside the bubble respectively. f_{air} and f_{water} are the capillary forces at distance d of a fluid bridge inside and outside the bubble surrounded by air and water respectively , and f_{bubble} is the capillary force contribution due to the bubble meniscus alone.

The capillary force, f is the sum of two contributions: surface tension and Laplace pressure. Force versus distance for a single capillary bridge is calculated by numerical simulations, described in appendix (A.1) and used to obtain F_{net} as a function of d for each type of contact. The adhesion force of the full hairy pad system is then obtained from the minima of the respective force-distance curves.

We have considered f_{air} and f_{water} to be distinct terms because the capillary force by the adhesive fluid will be different in air and water due to its different contact angles and interfacial tensions. Using the Young-Dupre equations, one can derive the following relation

for the contact angle of the adhesive fluid underwater:

$$\cos\theta_{fw} = \frac{\gamma_{fa}\cos\theta_{fa} - \gamma_{wa}\cos\theta_{wa}}{\gamma_{fw}} \tag{3}$$

Here, ϑ_{fw} and ϑ_{fa} are the contact angles of the adhesive fluid with the substrate in water and air respectively, ϑ_{wa} is the contact angle of water with the substrate in air, γ_{fa} is the surface tension of adhesive fluid, γ_{wa} is the surface tension of water and γ_{fw} is the interfacial tension of adhesive fluid with water.

All lengths are normalized w.r.t. s_f and forces are normalized w.r.t. $\gamma_{fa}s_f$.

Fixed parameter values used for all model calculations are given in ▤ We consider representative hydrophilic and hydrophobic substrates with ϑ_{fa} and ϑ_{wa} values corresponding to a typical glass and fluorinated surface respectively. We assume the adhesive fluid to be an oil-lke substance and thus the interfacial tension ratios γ_{wa}/γ_{fa} and γ_{fw}/γ_{fa} are taken corresponding to typical values of oil and water. Area fraction of hairs relative to the pad defined as $\alpha = ND_h{}^2/D_p{}^2$, hair aspect ratio L/D_h and fluid size parameter ϕ_f are fixed to values typical for an insect hairy pad.

First ▤ we calculate force-distance curves for a single pinned liquid capillary bridge. Secondly, the effect of substrate on the resultant force-distance curve of the hairy pad system is studied for each type of contact. Thirdly, the effect of varying hair diameter on net adhesion is studied by varying D_p/D_h. Finally, ϕ_b is varied to study the effect of bubble volume on the net underwater adhesion.

Table 4: Model parameters

Property	Value
Area fraction, α	0.1
Hair aspect ratio, L/D_h	10
Water surface tension, γ_{wa}/γ_{fa}	3
Fluid-Water interfacial tension, γ_{fw}/γ_{fa}	2
Fluid size parameter, ϕ_f	2
Hydrophilic substrate	$\theta_{fa}{=}6°$, $\theta_{wa}{=}24°$
Hydrophobic substrate	$\theta_{fa}{=}50°$, $\theta_{wa}{=}120°$

3.2 Results

3.2.1 Capillary force of a pinned liquid bridge

Forces due to a single pinned capillary liquid bridge in contact with a substrate are obtained via simulations (Figure 4). Capillary forces are more attractive for smaller contact angles. The Laplace pressure contribution to the net adhesion force dominates for contact angles less than 100° (Figure 4b). Interestingly, its contribution to adhesion force is mostly non-repulsive for contact angles greater than 90°. This is because the low volume of fluid and pinned contact line prevents the fluid bridge from having a high positive curvature due to geometric constraints. Only for a contact angle of 150° ~~does~~ the fluid curvature become positive, manifested in its slightly repulsive Laplace contribution. Surface tension makes a significant contribution to the net force only for ~~high~~ contact angles greater than 70°. For contact angles greater than 150°, the net adhesive force approaches zero. Since Laplace pressure is an indicator of the fluid bridge shape, one can make a general statement that the shape of the fluid bridge primarily determines the strength of its adhesion force for low and high contact angles. High adhesion is thus seen for contact angles less than 70° due to a net negative curvature of the fluid shape, while low adhesion is seen for contact angles greater than 150° due to its net curvature being close to zero.

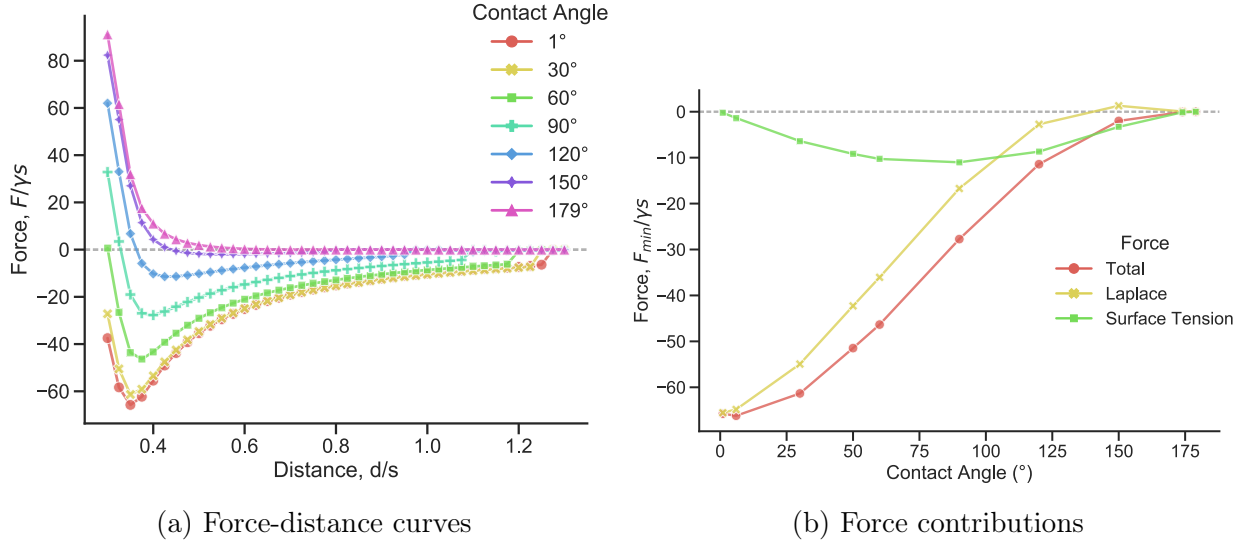(a) Force-distance curves   (b) Force contributions

Figure 4: Normalized capillary force of a single liquid meniscus in contact with a substrate ~~below~~ and pinned to a circular perimeter on top. Fluid size parameter $\phi_f = 2$. Negative value represents attractive for̲ a) Force-distance curves are shown for different contact angles of the liquid with the substrate̲ Adhesion force, calculated from the minima of the corresponding force-distance curve ~~is~~ plotted as a function of contact angle with̲ bstrate. Laplace̲ d surface tension contributions to the net total adhesion force are ~~also~~ show̲

The force-distance curves show a general trend of being repulsive at small distances (Figure4 a). This is a result of the pinned contact line constraint. A limited volume is available for the fluid to occupy when the gap distance is lo̲ ausing the fluid shape to bulge outward near the pinned contact line. This creates a net positive curvature, resulting in a positive Laplace pressure and thus repulsion.

3.2.2 Capillary Bridge Model: Effect of̲ bstrate

The normalized force-distance curves for a hairy pad system on a hydrophilic and hydrophobic substrate are predicted based on̲ pillary Bridge Model (Figure 5). The forces for each type of contact are calculated from equations (1) and (2). Rest of the parameters are kept constant for a direct comparison of the effect of contact type and substrate chemistry.

On the hydrophilic substrate̲ ontact in air shows the highest attractive forces. ~~In~~ underwater, the "wet" contact shows close to no adhesion while "bubble" contact shows

moderate adhesion. In contrast, for a hydrophobic substrate, the highest attractive forces are seen in underwater "wet" contact, much larger than adhesion in air. Even underwater "bubble" contact has slightly higher adhesion than in air. Note that we have eliminated the effect of contact area by fixing the area fraction α and pad/hair size (D_p/D_h). All curves correspond to the same total hair contact area. The above effects can thus be attributed solely to how capillary force changes for each type of contact.

On a hydrophilic substrate, the contact angle of the oily adhesive fluid is 6° (Table 4) when surrounded by air and 150° when surrounded by water, as calculated from equation (3). This results in the capillary bridge shape having a net negative and slightly positive curvatures respectively (Figure 8). Since Laplace contribution controls capillary force at such extreme contact angles (see section 3.2.2), the fluid bridges show strong adhesion in air while underwater, it shows little to no adhesion.

On a hydrophobic substrate however, the contact angles of the fluid in air and water are 50° and 1° respectively. In both cases, the contact angles are low, resulting in a net attractive force in both types of contact. Additionally, the interfacial tension of the oily fluid underwater (γ_{fw}) is twice that of in air (γ_{fa}). Thus, we see higher attractive force in an underwater "wet" contact when compared to contact in air.
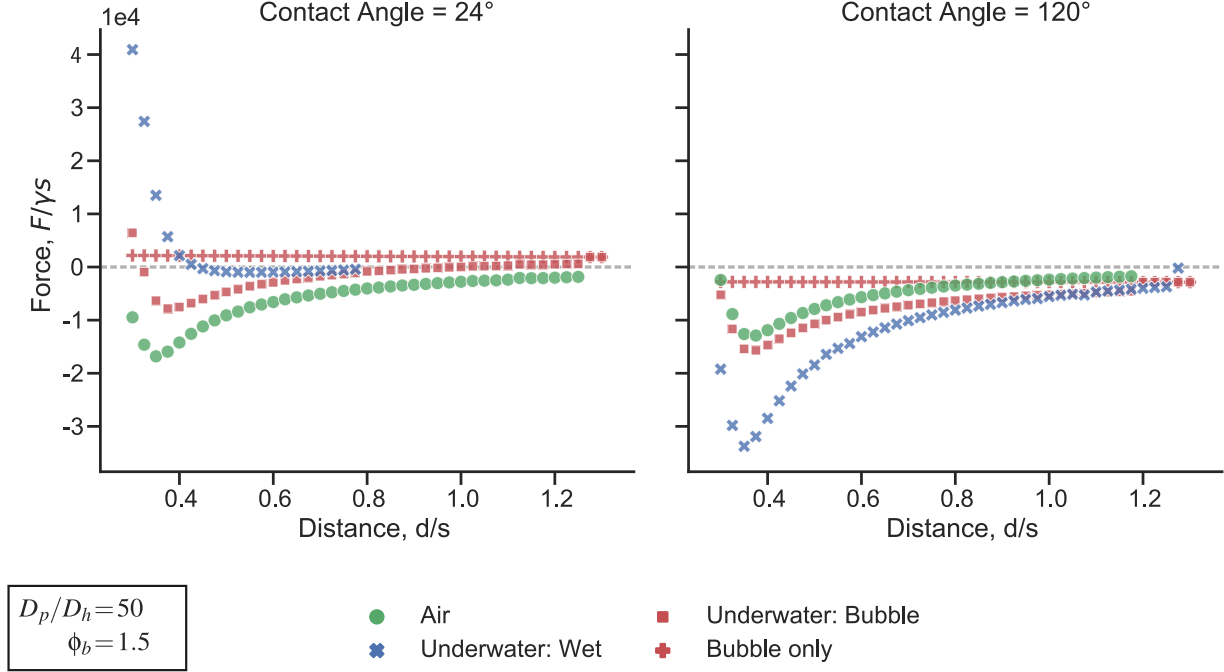
18

Figure 5: Theoretical force-distance curves of a hairy pad system on a hydrophilic (left) and hydrophobic (right) substrate in air and underwater conditions. [negative] ative value represents attractive force. Normalized forces are calculated from Capillary Bridge Model, with model parameters listed in Table 4. The bubble's contribution to the net force for an "Underwater: Bubble" contact is denoted by plus symbols. Pad to hair size ratio (D_p/D_h) and bubble size parameter (ϕ_b) are kept fixed

The net force in the underwater "bubble" contact mainly depends on the proportion of hairs ~~that are~~ inside the bubble surrounded by air or outside the bubble surrounded by water (see equation (2)). For the given bubble size (parameter ϕ_b), only part of the hairs are inside the bubble for the hydrophilic substrate while all the hairs are inside the bubble for the hydrophobic substrate. ~~This is why~~ its force curve lies in between air and underwater "wet" contact on a hydrophilic substrate, and closely follows air contact for hydrophobic substrate.

The contribution of capillary force created by the bubble alone to the net adhesion in underwater "bubble" contact is negligible for both hydrophilic and hydrophobic substrates (Figure 5). Its contribution is slightly repulsive on the hydrophilic substrate due to the positive curvature of the bubble, and slightly attractive on the hydrophobic substrate due to its negative curvature. This small contribution is manifested by a small downward shift

in the underwater "bubble" contact force curve on hydrophobic substrate. Here, all the hairs are trapped inside the bubble and thus its slightly higher adhesion relative to air contact is due to the small additional contribution of the bubble.

3.2.3 Capillary Bridge Model: Effect of hair diameter

The effect of changing hair diameter, D_h to the net adhesion force is compared for hydrophilic and hydrophobic substrates (Figure 6). Here, the pad diameter, total hair contact area and bubble volume are constant since D_p, α and ϕ_b are fixed. Fluid volume is assumed to scale in a self-similar manner by varying the effective fluid size proportional to the hair diameter ($\phi_f = 2$)

Adhesion force increases with decreasing D_h for both hydrophilic and hydrophobic substrates in all contact types. This is consistent with the "contact splitting" theory which predicts higher adhesion on splitting contacts to smaller size[20]. Reducing the hair diameter results in two competing effects: 1) capillary force due to a single fluid bridge decreases due to its smaller size and self-similar scaling assumption, which decreases the net force, and 2) total number of fluid bridges, N increases since the total hair contact area is assumed to be fixed, which increases the net force. The net effect results in higher adhesion force as D_h is decreased.
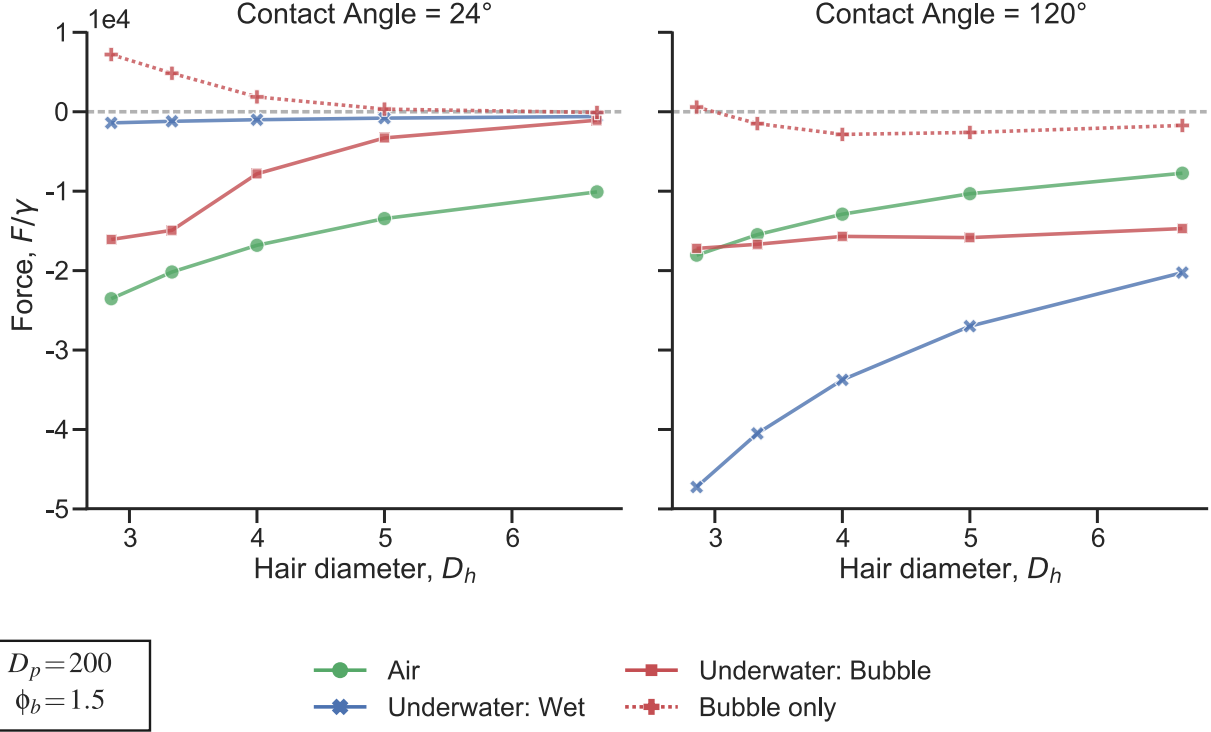
Figure 6: Normalized adhesion force of hairy pad system on a hydrophilic (left) and hydrophobic (right) substrate as a function of pad to hair diameter (D_h), calculated from Capillary Bridge Model. Negative value represents attractive force. The bubble's contribution to the net force for an "Underwater: Bubble" contact is denoted by plus symbols. Pad diameter and bubble size parameter (ϕ_b) are kept fixed to 200 and 1.5 respectively. Adhesion forces are calculated from minima of the respective force-distance curves. Length is in arbitrary units.

Similar to the trend in Figure 5, contact in air shows the highest adhesion force for the hydrophilic substrate for all hair sizes, while on the hydrophobic substrate, underwater "wet" contact shows highest adhesion. Underwater "bubble" contact shows intermediate adhesion between air and underwater "wet" contact types.

The bubble ~~only~~ contribution to underwater "bubble" contact gets repulsive as hair size is decreased for both substrates (Figure 6). Since the aspect ratio L/D_h is fixed (Table 4), decreasing the hair size also decreases its length. The bubble has less space available between the pad and the substrate, resulting in it bulging outwards near the pinned contact line on top. Thus, bubble contribution gets repulsive as hair size decreases if bubble size is kept constant.

3.2.4 Capillary Bridge Model: Effect of bubble volume

The effect of varying bubble size parameter ϕ_b on the net adhesion force of the underwater "bubble" contact for hydrophilic and hydrophobic substrates are compared (Figure 7). Increasing ϕ_b implies smaller bubble volume and thus larger proportion of fluid bridges outside the bubble. From section 3.2.2, we know that on the hydrophilic substrate, fluid bridges outside the bubble contributes very little adhesion due to its positive curvature. Thus, decreasing the bubble volume decreases adhesion force due to the larger proportion of hairs outside the bubble. In contrast, on the hydrophobic substrate, fluid bridges outside the bubble haves a stronger contribution to the net capillary force due to the low contact angle and high interfacial tension in water. Thus, adhesion force increases for a hydrophobic substrate as bble size decreases.
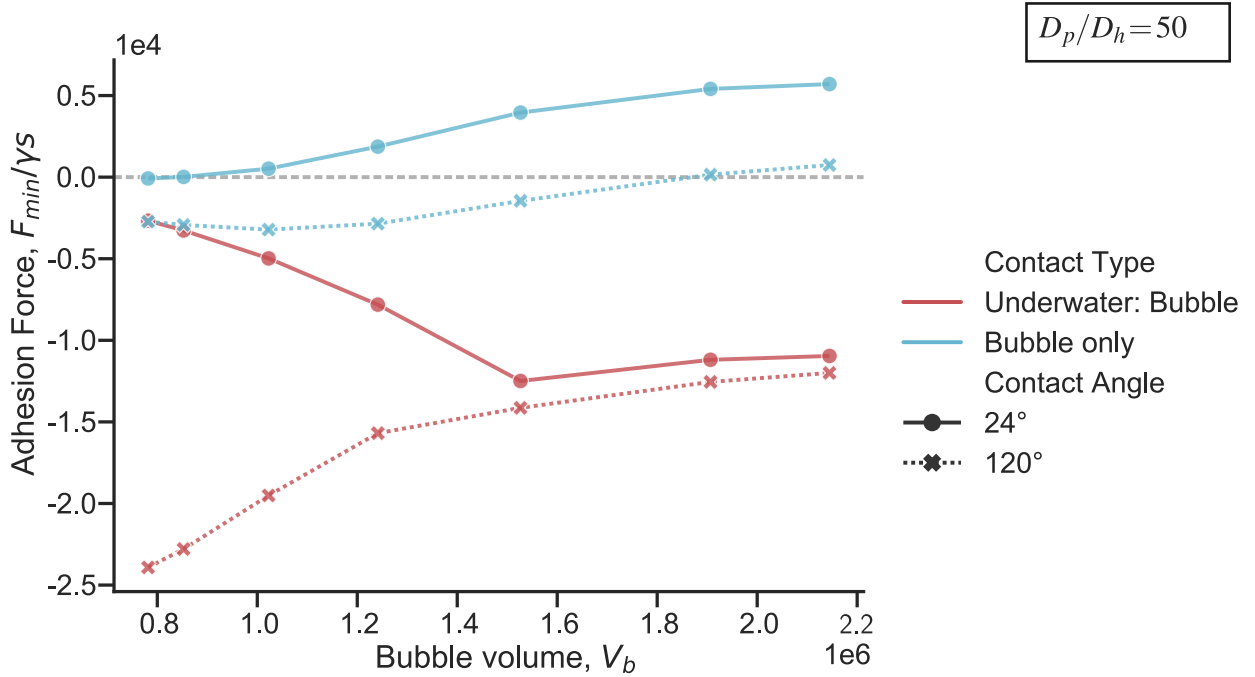

Figure 7: Normalized adhesion force of ry pad system as a function of bubble size parameter (ϕ_b) for "Underwater: Bubble" contact type (red). Negative value represents attractive force. Higher ϕ_b value implies a smaller bubble size. Bubble's contribution to the net adhesion is shown in blue. Here, pad to hair size ratio (D_p/D_h) is kept fixed. Adhesion forces are calculated from minima of the respective force-distance curves.

Bubble's capillary contribution to the net adhesion force is small regardless of its size.

22

We see that a smaller bubble (large ϕ_b) tends towards more attraction by the bubble in both kind of substrates, though negligibly. For small values of ϕ_b, the net underwater "bubble" contact force mostly follows the "bubble only" contribution, because the bubble in this case is big enough to entrap all hairs inside it. Thus initially, the force contribution due to the fluid bridges remain flat while the bubble contribution increases slightly as ϕ_b increases. Once the bubble gets small enough and part of the fluid bridges make contact in water, the force trend changes with a steep decrease or increase in adhesion force on hydrophilic and hydrophobic substrates respectively.

To summarize, on a hydrophilic substrate, a trapped air bubble in the adhesive pad can promote adhesion when its large enough to enclose most of the hairs which allows for contact in an air environment. This is because "wet" hairs underwater show no adhesion due to the fluid's large contact angle and the only way to achieve adhesion is by maintaining the hairs in the air environment provided by the bubble. On a hydrophobic substrate however, a smaller or no bubble enhances adhesion, as the bubble has little effect on improving adhesion force. Here, hairs making a "wet" contact underwater show stronger adhesion than in air due to the fluid's smaller contact angle and higher interfacial tension. In either case, the bubble by itself hardly contributes to the net force. Despite its large size, the bubble fails to overcome the combined contribution of the much smaller fluid bridges to the total force.

4   Discussion

Our experiments demonstrate for the first time that the ladybug beetle can attach to a hydrophobic substrate even without a bubble trapped around its hairs. A previous study [17] had hypothesized that bubble is necessary for underwater attachment in beetles. This is however only true for glass substrates where only the underwater "bubble" contact shows significant adhesion while "wet" contact shows poor adhesion. For a hydrophobic substrate, all forces lie in a similar range regardless of the type of contact, with the only exception of

"bad contact".

Experimental results are in qualitative agreement with the predictions from Capillary Bridge Model (Figure 2). Here, we set the model parameters to resemble a ladybug's distal pad. On PFOTS, "wet" contact shows adhesion similar to dry contact in air, while on ss, "wet" contact has very low adhesion. This is explained by the different oil contact angles and interfacial tension for these two substrates in air and underwater conditions (Figure 8). The measurements however don't show a significantly higher adhesion for the underwater "wet" contact on PFOTS when compared to its adhesion in air as predicted by the model. This could be due to the additional complexity involved in making a good underwater contact. We already observe that "bad contact" can lead to complete loss of adhesion. It is thus possible that such bad contacts are happening locally for some hairs which reduces the net adhesion force for the "wet contact".
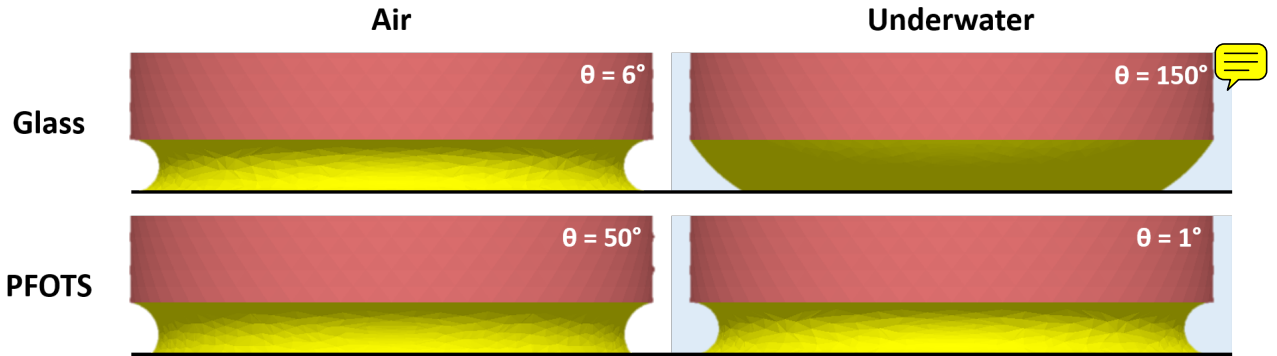

Figure 8: Simulation snapshots of oil capillary meniscus in contact with glass and PFOTS in air and underwater conditions

The role of bubble for underwater adhesion is further clarified based on the model. The bubble by itself has a negligible capillary contribution to the net adhesion force underwater. Bubble can only help in adhesion on a hydrophilic substrate by providing the hairs an air environment such that the liquid capillary bridges show adhesion similar to that in air. For a hydrophobic substrate, having a trapped bubble has no significant effect on improving adhesion as even a "wet" contact underwater shows adhesion similar to that in air.

The model assumes a perfect contact of each hair which detaches simultaneously to give

a theoretical maximum adhesion force achievable. Our experimental conditions are however far from such assumptions. The pad always makes a partial contact with the substrate at a random angle, which is difficult to control precisely. During detachment, the pad typically peels off from its proximal to distal end rather than detach simultaneously. Our model also assumes the hairs to be perfectly rigid and of similar geometry unlike reality. Thus it's not surprising that the model overestimates the adhesion forces. The predictions are however in the same order of magnitude as experiments, and the qualitative trend is consistent for both hydrophilic and hydrophobic substrates in air and underwater.

Our study provides further validation that capillary forces by the adhesive fluid control insect adhesion and van der Waals contribution, if any, must be negligible. For underwater "wet" contact, the pad adheres strongly to a PFOTS substrate, but poorly to a glass substrate even though it shows similarly strong adhesion to both substrates in air. This behavior can only be explained by capillary forces.

Our findings can also be extended to other animals relying on oily adhesive fluids for adhesion. Ants for example show similar adhesion on hydrophobic substrates under wet and dry conditions[21], similar to what we see in a ladybug. Recent adhesion experiments on geckos reveal that it can attach well to fluoropolymer substrates underwater while shows little adhesion to the same substrate in air[15,16]. Although a work of adhesion model assuming dry contact is able to explain this result qualitatively, the same model fails to predict the low underwater adhesion seen for the slightly hydrophilic substrates such as PMMA or PET. Geckos are thought to rely on van der Waals forces via dry contact with the substrate[6], although recent observations of phospholipid footprints left behind walking geckos[22] could change that picture. Since geckos adhere poorly to PTFE (surface energy ~ 20 mN/m) one can speculate that the phospholipid material has a higher surface energy, and consequently makes a higher contact angle with PTFE in air. Let us assume the phosopholipid material to be a fluid similar to oil with γ_{fa}=30 mN/m and γ_{fw}= 42 mN/m such that its contact angle with PTFE is 80°. Equation 3 then gives us an underwater contact angle of 70° for

the phospholipid fluid. Thus, the Capillary Bridge Model can predict a higher adhesion underwater than in air with PTFE due to its lower contact angle and higher interfacial energy underwater. Based on similar assumptions, we predict the net adhesion force for a gecko on different substrates (Figure 9). The adhesion force predictions are in qualitative agreement with the whole animal experimental shear force values reported for the gecko, with the trend of higher adhesion in air than underwater for glass, similar adhesion in air and underwater for PMMA/OTS-SAM and lower adhesion in air than underwater for PTFE. We us pose that the underwater experiments performed on geckos[15,16] are an indirect proof of capillary contribution to gecko adhesion in this scenario. We suggest performing single seta adhesion force tests similar to Autumn et. al.[6] using a hydrophilic and fluorinated probe in air and underwater conditions to validate the role of capillary contributions to gecko adhesion.

We have so far limited our analysis to only smooth substrates. Insects in the real world wever eracts with rough substrates all the me. Previous studies[23] have shown that substrate roughness is a more dominant parameter than substrate chemistry in controlling insect adhesion. Future work will explore how roughness can impact the net capillary force as predicted by our model. Our study can have potential applications in the design of bioinspired materials to achieve adhesion via capillary bridges. Bubble can be possibly be used to control underwater adhesion by changing the relative proportion of the arrays inside and outside the bubble. A suitable choice of adhesive fluid can be made tailored to the substrate and environment of application for optimal adhesion performance. Future studies on insect adhesion should characterize oleophilicity rather than hydrophilicity of a substrate, since oil contact angle primarily controls its adhesion to the substrate.
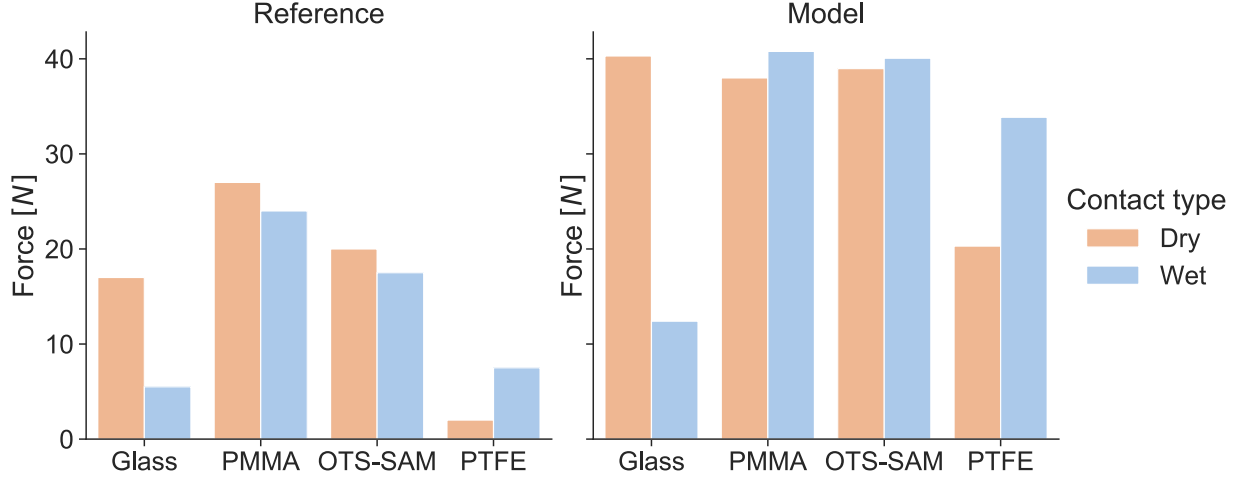
Figure 9: Whole animal adhesion force of gecko on various substrates. Experimental shear adhesion values are reproduced from Stark et. al.[15]. Normal adhesion forces for each gecko toe are theoretically estimated from Capillary Bridge Model, with hair diameter = 400 nm, toe diameter = 4 mm, adhesive fluid volume = 4.19x10^{-3} fL and 10% hair coverage. "Underwater:Wet" contact is assumed for "Wet" contact. Net adhesion force is calculated by assuming 5 toes on each leg and 4 legs in total on a gecko. Interfacial tension of phospholipid layer (PL) in air and water are assumed to be 30 mN/m and 42 mN/m respectively. PL contact angles with glass, PMMA, OTS-SAM and PTFE are assumed to be 6°, 10°, 20° and 80° respectively. The corresponding water contact angles are 50°, 85°, 94° and 97° respectively, as reported in Stark et. al.[15].

5 Conclusions

Our study illustrates that ladybug relies primarily on its oily adhesive fluid secretion to achieve adhesion in both air and underwater conditions. We show ~~for the first time~~ that the beetles can attach underwater on a hydrophobic substrate even without a trapped air bubble within its hairy pad, although it loses this ability on a hydrophilic substrate. The different contact angle and interfacial tension manifested by the adhesive fluid in air and underwater conditions explains this observation. Theoretical calculations suggest that the bubble itself has a negligible capillary contribution to the total force. The trapped bubble can promote adhesion only on a hydrophilic substrate by providing an air medium to the adhesive fluid bridges inside it ~~in contact with the substrate~~. Insect adhesion is ~~thus~~ correlated directly to the shape of the adhesive fluid on a given substrate and medium, which is a result of

27

the small fluid volume and its contact angle with the substrate. A similar argument can also consistently explain previously reported measurements in geckos [15], which highlights the possibility of capillary contributions to gecko adhesion

6 Acknowledgement

A Appendix

A.1 Simulation method: Single capillary bridge

Capillary force due to a single adhesive fluid or bubble meniscus ("capillary bridge") is calculated by performing simulations in Surface Evolver [24], similar to the method described in De Souza et. al. [25]. A simple cubic geometry mimicking the capillary bridge of constant volume V is defined as the initial condition with an interfacial tension γ with the surrounding medium. Interfacial tension of the capillary bridge with the substrate is given by $\gamma\cos\vartheta$, where ϑ is the corresponding contact angle inside the bridge. For the case of a bubble meniscus, ϑ is defined w.r.t. the surrounding water since ϑ can also then characterize the substrate wettability. The capillary bridge spans a gap distance d between the top face and the substrate. The boundary conditions are set corresponding to a pinned contact line of diameter D on the top face and constant interfacial tension with the substrate on the bottom. All lengths are normalized relative to length s = $(3V/4\pi)^{1/3}$. An appropriate geometry refinement routine is chosen to evolve the capillary bridge shape to its minimum energy state. The normalized total capillary force, F=f/γs, is the sum of the Laplace pressure and surface tension contributions , where:

$$f = f_{laplace} + f_{surface\,tension} = \Delta P_{laplace} A_{bottom} + 2\pi R_{bottom} \gamma \sin \theta \qquad \text{(A.1)}$$

Here, $\Delta P_{laplace}$ which is the Laplace pressure of the equilibrium capillary bridge, A_{bottom} which is the contact area of the capillary bridge with the substrate at bottom and R_{bottom} which is the corresponding radius of contact are all obtained from the simulation output for the equilibrium surface.

The gap distance d is varied by fixed steps and the capillary force is calculated each time to obtain force-distance curves for a particular choice of D and ϑ.

A.2   Single capillary bridge: Effect of volume

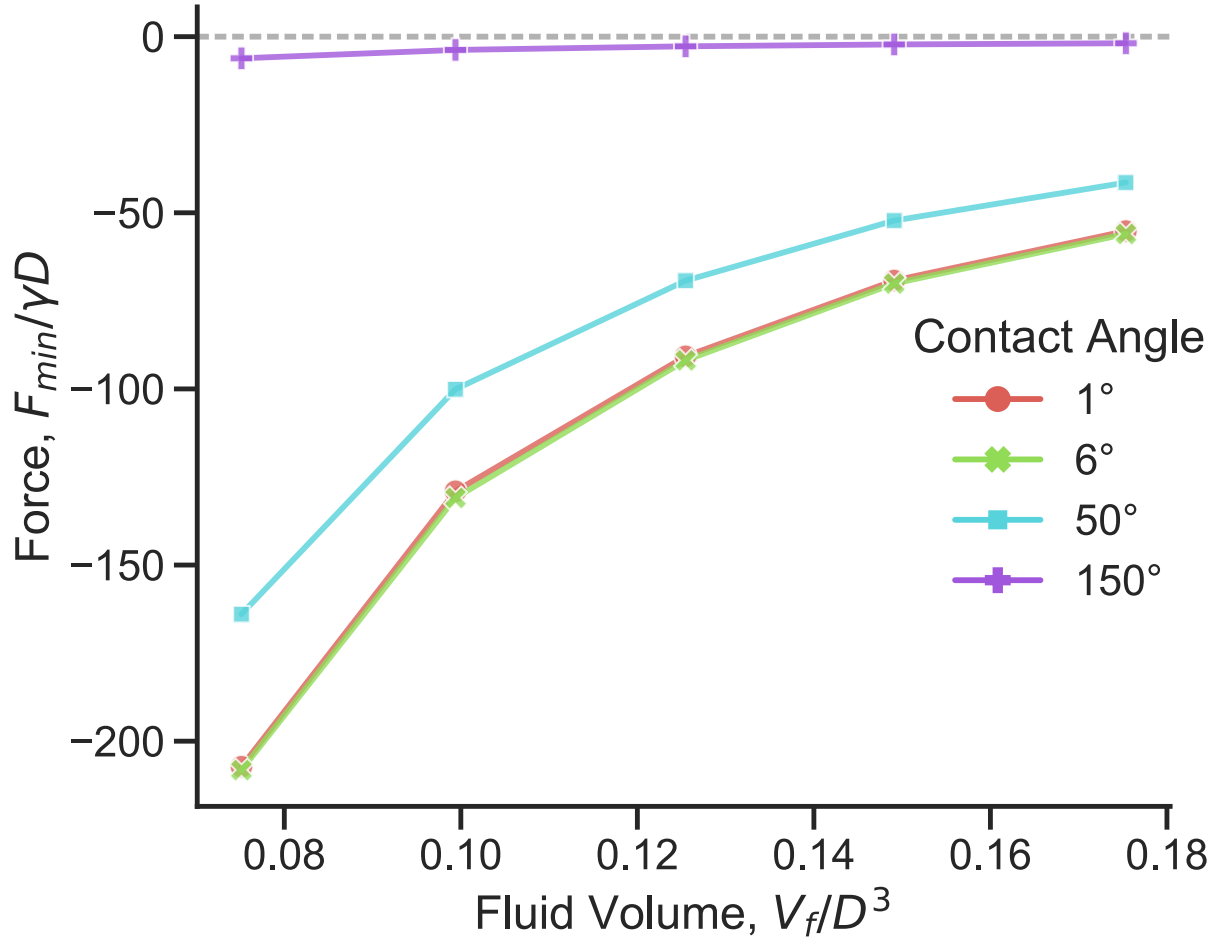Below plot show the effect of volume on the maximum capillary force of a single fluid bridge.

Figure A.1: Normalized maximum capillary force as a function of fluid volume

A.3 Capillary Bridge Model: Effect of hair diameter at constant fluid volume

Here, instead of assuming a self-similar scaling of fluid volume, we assume a fixed total fluid volume distributed equally among the N hairs. Hair diameter is varied while keeping the total hair contact area constant. Length is arbitrary units. Forces increase at a much smaller rate on decreasing diameter when compared to the case with self-similar scaling of fluid volume.
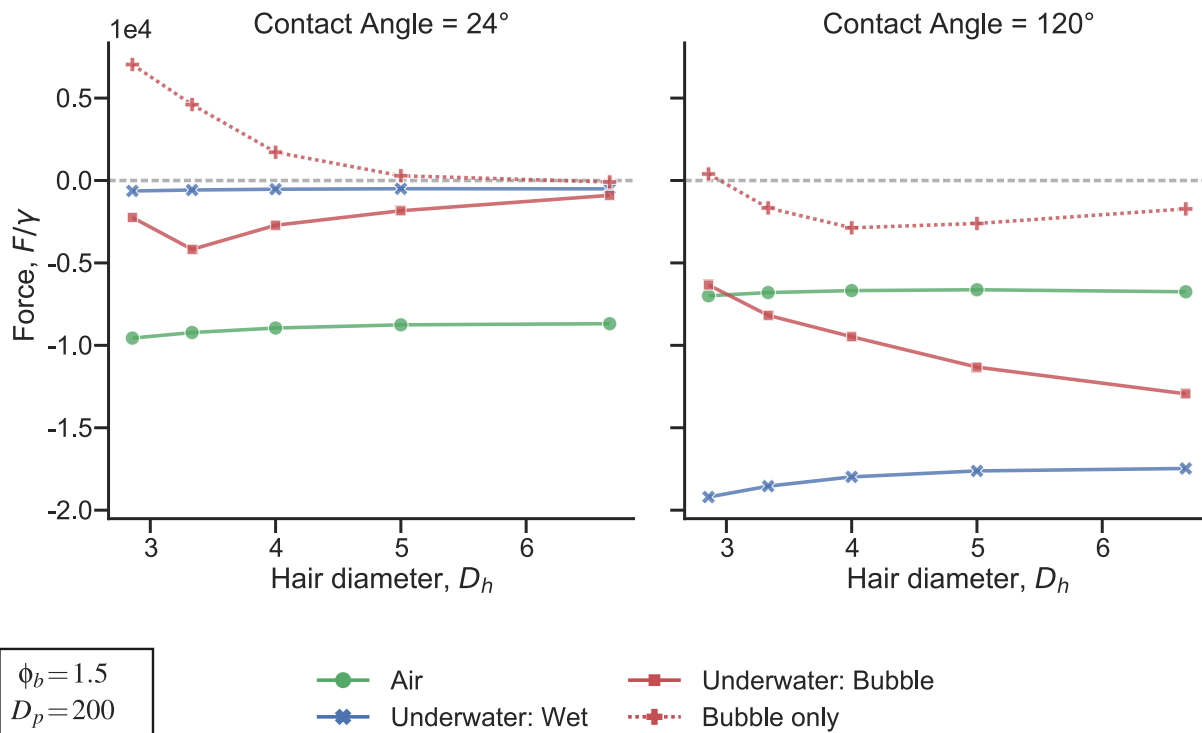
Figure A.2: Normalized adhesion force of hairy pad system on a hydrophilic (left) and hydrophobic (right) substrate as a function of hair diameter (D_h), calculated from Capillary Bridge Model. Negative value represents attractive force. The bubble's contribution to the net force for an "Underwater: Bubble" contact is denoted by plus symbols. Bubble size parameter (ϕ_b), pad diameter ($D_p = 200$) and total adhesive fluid volume ($NV_f = 2000$) are kept fixed. Adhesion forces are calculated from minima of the respective force-distance curves.

References

(1) Hooke, R. *Micrographia, or, Some physiological descriptions of minute bodies made by magnifying glasses : with observations and inquiries thereupon*; The Royal Society, 1665.

(2) Stork, N. E. Experimental Analysis of Adhesion of Chrysolina Polita (Chrysomelidae: Coleoptera) on a Variety of Surfaces. *The Journal of Experimental Biology* **1980**, *88*, 91.

(3) Federle, W. Why are so many adhesive pads hairy? *J Exp Biol* **2006**, *209*, 2611–21, DOI: `10.1242/jeb.02323`.

(4) Federle, W.; Riehle, M.; Curtis, A. S.; Full, R. J. An Integrative Study of Insect Adhesion: Mechanics and Wet Adhesion of Pretarsal Pads in Ants. *Integrative and Comparative Biology* **2002**, *42*, 1100–1106, DOI: `10.1093/icb/42.6.1100`.

(5) Dirks, J. H. Physical principles of fluid-mediated insect attachment - Shouldn't insects slip? *Beilstein J Nanotechnol* **2014**, *5*, 1160–6, DOI: `10.3762/bjnano.5.127`.

(6) Autumn, K.; Sitti, M.; Liang, Y. A.; Peattie, A. M.; Hansen, W. R.; Sponberg, S.; Kenny, T. W.; Fearing, R.; Israelachvili, J. N.; Full, R. J. Evidence for van der Waals adhesion in gecko setae. *Proceedings of the National Academy of Sciences* **2002**, *99*, 12252, DOI: `10.1073/pnas.192252799`.

(7) Bullock, J. M.; Federle, W. Division of labour and sex differences between fibrillar, tarsal adhesive pads in beetles: effective elastic modulus and attachment performance. *J Exp Biol* **2009**, *212*, 1876–88, DOI: `10.1242/jeb.030551`.

(8) Bullock, J. M.; Federle, W. Beetle adhesive hairs differ in stiffness and stickiness: in vivo adhesion measurements on individual setae. *Naturwissenschaften* **2011**, *98*, 381–7, DOI: `10.1007/s00114-011-0781-4`.

(9) Peisker, H.; Gorb, S. N. Evaporation dynamics of tarsal liquid footprints in flies (Calliphora vicina)and beetles (Coccinella septempunctata). *The Journal of Experimental Biology* **2012**, *215*, 1266–1271, DOI: `10.1242/jeb.065722`.

(10) Geiselhardt, S. F.; Geiselhardt, S.; Peschke, K. Comparison of tarsal and cuticular chemistry in the leaf beetle Gastrophysa viridula (Coleoptera: Chrysomelidae) and an evaluation of solid-phase microextraction and solvent extraction techniques. *Chemoecology* **2009**, *19*, 185, DOI: `10.1007/s00049-009-0021-y`.

(11) Attygalle, A. B.; Aneshansley, D. J.; Meinwald, J.; Eisner, T. Defense by foot adhesion in a chrysomelid beetle (Hemisphaerota cyanea): characterization of the adhesive oil. *Zoology* **2000**, *103*, 1–6.

(12) Ishii, S. Adhesion of a Leaf Feeding Ladybird Epilachna vigintioctomaculta (Coleoptera : Coccinellidae) on a Virtically Smooth Surface. *Applied Entomology and Zoology* **1987**, *22*, 222–228, DOI: `10.1303/aez.22.222`.

(13) Gernay, S.; Federle, W.; Lambert, P.; Gilet, T. Elasto-capillarity in insect fibrillar adhesion. *J R Soc Interface* **2016**, *13*, DOI: `10.1098/rsif.2016.0371`.

(14) Ditsche, P.; Summers, A. P. Aquatic versus terrestrial attachment: Water makes a difference. *Beilstein Journal of Nanotechnology* **2014**, *5*, 2424–2439, DOI: `10.3762/bjnano.5.252`.

(15) Stark, A. Y.; Badge, I.; Wucinich, N. A.; Sullivan, T. W.; Niewiarowski, P. H.; Dhinojwala, A. Surface wettability plays a significant role in gecko adhesion underwater. *Proc Natl Acad Sci U S A* **2013**, *110*, 6340–5, DOI: `10.1073/pnas.1219317110`.

(16) Stark, A. Y.; Dryden, D. M.; Olderman, J.; Peterson, K. A.; Niewiarowski, P. H.; French, R. H.; Dhinojwala, A. Adhesive interactions of geckos with wet and dry fluoropolymer substrates. *Journal of The Royal Society Interface* **2015**, *12*, 20150464, DOI: `doi:10.1098/rsif.2015.0464`.

(17) Hosoda, N.; Gorb, S. N. Underwater locomotion in a terrestrial beetle: combination of surface de-wetting and capillary forces. *Proc Biol Sci* **2012**, *279*, 4236–42, DOI: `10.1098/rspb.2012.1297`.

(18) Peattie, A. M.; Dirks, J.-H.; Henriques, S.; Federle, W. Arachnids secrete a fluid over their adhesive pads. *PloS one* **2011**, *6*, e20485–e20485, DOI: `10.1371/journal.pone.0020485`.

(19) Sudersan, P. Buggee - An intergrative tool for synchronous data analysis, image processing and plotting. **2020**, DOI: `https://github.com/PranavSudersan/Buggee`.

(20) Arzt, E.; Gorb, S.; Spolenak, R. From micro to nano contacts in biological attachment devices. *Proc Natl Acad Sci U S A* **2003**, *100*, 10603–6, DOI: `10.1073/pnas.1534701100`.

(21) Stark, A. Y.; Yanoviak, S. P. Adhesion and running speed of a tropical arboreal ant (Cephalotes atratus) on wet substrates. *Royal Society open science* **2018**, *5*, 181540–181540, DOI: `10.1098/rsos.181540`.

(22) Hsu, P. Y.; Ge, L.; Li, X.; Stark, A. Y.; Wesdemiotis, C.; Niewiarowski, P. H.; Dhinojwala, A. Direct evidence of phospholipids in gecko footprints and spatula - substrate contact interface detected using surface-sensitive spectroscopy. *Journal of The Royal Society Interface* **2012**, *9*, 657–664, DOI: `doi:10.1098/rsif.2011.0370`.

(23) England, M. W.; Sato, T.; Yagihashi, M.; Hozumi, A.; Gorb, S. N.; Gorb, E. V. Surface roughness rather than surface chemistry essentially affects insect adhesion. *Beilstein journal of nanotechnology* **2016**, *7*, 1471–1479, DOI: `10.3762/bjnano.7.139`.

(24) Brakke, K. A. The surface evolver. *Experiment. Math.* **1992**, *1*, 141–165.

(25) De Souza, E. J.; Brinkmann, M.; Mohrdieck, C.; Arzt, E. Enhancement of Capillary Forces by Multiple Liquid Bridges. *Langmuir* **2008**, *24*, 8813–8820, DOI: `10.1021/la8005376`.